Design and Optimization of Superconducting MRI Magnet Systems With Magnetic Materials

Tony Tadic and B. Gino Fallone

***Abstract*—We present a method for the optimal design of superconducting magnet systems for magnetic resonance imaging (MRI). The method integrates a linear-programming technique with the finite-element method (FEM) to calculate minimum-volume coil configurations subject to magnetic field homogeneity constraints for MRI systems that contain general nonaxisymmetric magnetic yoke structures. The method rapidly converges and only requires a small number of iterations and FEM analyses to be performed. In particular, the method is well suited for magnet design problems that necessitate large 3-D FEM models. We demonstrate the method with the optimal design of an open and compact 0.5 T yoked biplanar magnet assembly considered for use in an integrated medical linear accelerator and MRI system. In particular, the coil configuration for this magnet design is constructed from a MgB_2 high-temperature superconducting material that operates in a conduction-cooled cryogen-free environment.**

***Index Terms*—Image-guided radiation therapy, magnet design, magnetic resonance imaging (MRI), optimization, superconducting magnets.**

I. Introduction

SUPERCONDUCTING magnet systems are currently the most widely used magnet types for generating the strong homogeneous static magnetic field required for clinical magnetic resonance imaging (MRI). These systems are capable of greater field strengths, better temporal stability, and higher field uniformity than their permanent and resistive magnet counterparts. These highly advantageous features permit faster imaging, greater spatial resolution, and superior image quality.

The optimal design of superconducting MRI magnets has been the subject of considerable research. Many approaches that focus on the optimization of coil configurations to yield compact shielded magnets that exhibit a high degree of uniformity and confined fringe fields have been reported [1]–[11]. Despite yielding significantly different coil arrangements, the majority of the magnet designs resulting from these methods achieve similar performance [12]. Consequently, there has been a recent thrust to further develop techniques that also minimize the conductor volume of the coil configuration [13]–[25]. Because the cost of a superconducting magnet system is strongly related to the amount of the conductor used, this condition has become a growing factor of importance in the increasingly competitive market for MRI magnets.

The majority of optimization algorithms for superconducting magnets only consider designs that either have a cylindrical geometry [1], [25]–[34] or do not contain any magnetic materials [2]–[11], [13]–[24], thereby permitting a simplification of the required magnetic field analysis. This case was largely justified by the fact that most commercial full-body magnets satisfied these assumptions [12]. Field calculations for coil-only systems can rapidly be performed with formulas that are derived from the Biot–Savart law or by employing well-known spherical harmonic expansions [35]. When considering magnetized materials with nonlinear susceptibilities, the magnetic-field analysis becomes much more complicated. Equivalent magnetization current methods and other direct techniques utilizing analytical formulas for the magnetic fields due to magnetized rings have been proposed [29]–[32], although these schemes are strictly limited to cylindrical geometries. The finite-element method (FEM) has also been applied in problems that involve magnetic materials due to its high accuracy and ability to handle complicated geometries. However, to reduce the number of mesh elements and the associated computation time, the majority of optimization methods that employ the FEM assume simplified cylindrical geometries, permitting the use of smaller 2-D models [26]–[28], [33], [34].

Corresponding to the current trend toward improving patient access and decreasing patient claustrophobia, there is a growing demand for compact open biplanar magnet systems [12], [36], [37]. These magnets typically incorporate noncylindrical yoke structures, for which accurate analysis of the 3-D magnetic fields and associated inhomogeneities are required during the design process. We are therefore motivated to develop new optimization methods that can be applied to the design of these systems.

In this paper, we present an iterative method for the optimal design of homogenous superconducting magnet assemblies with general nonaxisymmetric magnetic yoke structures. A linear-programming (LP) subproblem is solved at each iteration to obtain a minimum-volume coil configuration while constraining the magnetic-field inhomogeneity within an arbitrary target volume [14]. The FEM is then used to calculate the complete 3-D magnetic field produced by the entire magnet

Manuscript received May 31, 2011; revised September 9, 2011; accepted November 27, 2011. Date of publication January 12, 2012; date of current version March 30, 2012. This paper was recommended by Associate Editor M. Parizh. This work was supported in part by Alberta Innovates–Health Solutions (AIHS) and the Natural Sciences and Engineering Research Council of Canada (NSERC).

T. Tadic is with the Medical Physics Department, Cross Cancer Institute, Edmonton, AB T6G 1Z2, Canada, and also with the Department of Physics, University of Alberta, Edmonton, AB T6G 2E1, Canada (e-mail: ttadic@gmail.com).

B. G. Fallone is with the Medical Physics Department, Cross Cancer Institute, Edmonton, AB T6G 1Z2, Canada, with the Department of Physics, University of Alberta, Edmonton, AB T6G 2E1, Canada, and also with the Department of Oncology, University of Alberta, Edmonton, AB T6G 1Z2, Canada (e-mail: gino.fallone@albertahealthservices.ca).

Color versions of one or more of the figures in this paper are available online at http://ieeexplore.ieee.org.

Digital Object Identifier 10.1109/TASC.2012.2183871

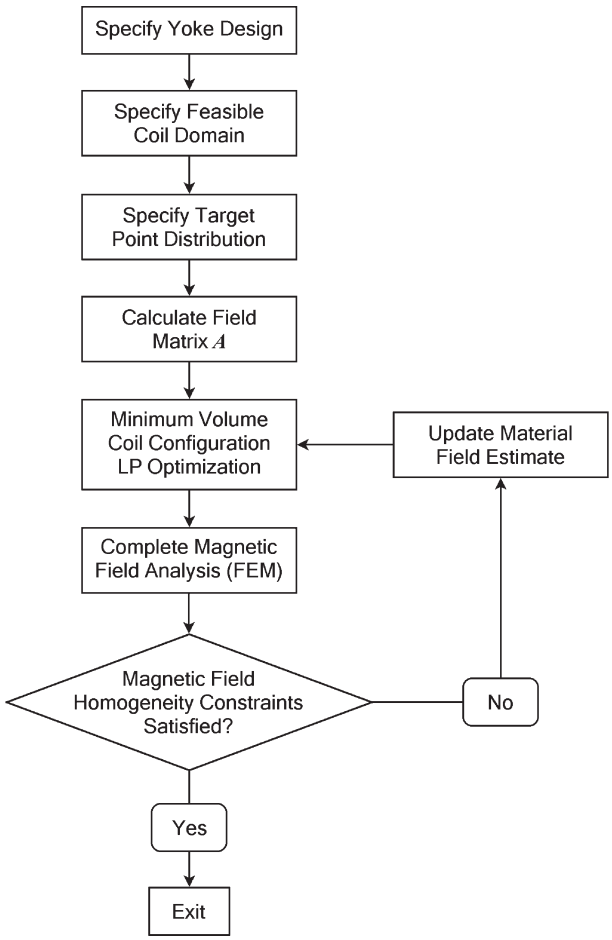

Fig. 1. Iterative optimization flow diagram.

system, thereby taking into account the presence of any magnetic materials. Our method exhibits good performance and typically requires a small number of iterations and FEM analyses to converge. Consequently, it is feasible to employ large 3-D FEM models that may require significant computation time due to high mesh densities or complicated geometries.

We demonstrate the effectiveness of the proposed method with the optimal design of an open compact 0.5 T biplanar superconducting magnet system with a four-column ferromagnetic yoke structure. A special feature of this magnet design is the use of a conduction-cooled cryogen-free coil assembly constructed from a MgB_2 high-temperature superconducting (HTS) material. Our group is considering the use of this magnet assembly in the design of an integrated medical linear accelerator (linac) and MRI system that can perform advanced real-time adaptive radiation therapy (ART^2) [38]–[40].

II. Optimization Method

A. Algorithm Overview

The ultimate goal of the method presented in this paper is to obtain minimum-volume coil configurations subject to magnetic field constraints for superconducting magnet systems that involve noncylindrical ferromagnetic yoke structures. This goal is achieved through the iterative optimization scheme summarized in the flow diagram in Fig. 1.

The design process begins with user specification of the magnetic yoke structure, for which the geometry and properties of the materials involved are held constant for all subsequent steps. The user then defines the feasible coil domain and a distribution of N_j target points at locations where the magnetic-field uniformity will be constrained. These points are typically chosen on the surface of a large diameter spherical volume (DSV) that is designated for imaging; thus, the constraints are expressed as

$$|b_j - B_0| \leq \varepsilon B_0 \qquad j = 1, \ldots, N_j \tag{1}$$

where b_j is the total axial component of the magnetic field at the target point j, B_0 is the desired magnetic field strength at the isocenter, and ε is the relative field error tolerance. The radial component of the magnetic field can be considered negligible when the axial component is homogenous [14]; therefore, it is not included in the constraint formulation.

It is assumed with this design method that the yoke structure itself provides adequate reduction of the magnetic fringe fields produced by the magnet assembly, as typically found with modern passively shielded biplanar MRI systems [12]. Consequently, we do not employ shielding constraints when optimizing the coil configuration.

For convenience, b_j can be separated into two components as

$$b_j = b_{cj} + b_{mj} \qquad j = 1, \ldots, N_j \tag{2}$$

where the coil field b_{cj} is the contribution strictly due to the free-current configuration, and the material field b_{mj} is the contribution due to the nonlinear magnetization induced in the magnetic materials. The target coil field b_{tj} can then be defined as

$$b_{tj} = B_0 - b_{mj} \qquad j = 1, \ldots, N_j \tag{3}$$

and the constraints (1) may be rewritten as

$$|b_{cj} - b_{tj}| \leq \varepsilon B_0 \qquad j = 1, \ldots, N_j. \tag{4}$$

A coil configuration is not initially defined, and thus, the magnetic field is zero at every target point, i.e.,

$$b_{cj}^{(0)} = b_{mj}^{(0)} = b_j^{(0)} = 0 \qquad j = 1, \ldots, N_j \tag{5}$$

where the superscript denotes the iteration number. Because the constraints (4) are not initially satisfied, the iterative design loop is engaged.

During the first step of each iteration, an LP method adapted from [14] is used to determine a minimum-volume coil arrangement such that (4) is satisfied. The details of this procedure are discussed in the following section. Because the true material field is unknown at this stage, the target coil field in (4) is calculated using the material field from the previous iteration as an estimate [27], [28]. Therefore, the coil configuration obtained with the LP method at the nth iteration satisfies

$$\left| b_{cj}^{(n)} - b_{tj}^{(n-1)} \right| \leq \varepsilon B_0 \qquad j = 1, \ldots, N_j \tag{6}$$

where the target coil field is given by

$$b_{tj}^{(n-1)} = B_0 - b_{mj}^{(n-1)} \qquad j = 1, \ldots, N_j. \tag{7}$$

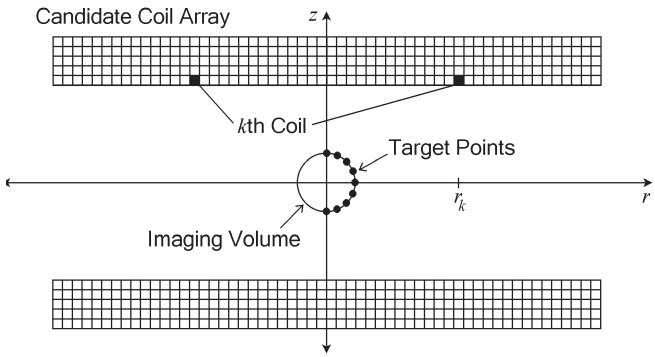

Fig. 2. Illustration of the feasible coil domain and target point distribution. The feasible coil domain is segmented by an array of candidate coils, shown here as centered on the z-axis. The target points at which the field homogeneity is constrained are typically distributed on the surface of a large DSV designated for imaging.

A FEM model that combines the new coil configuration with the specified yoke design is then generated, and the complete axial field at each of the target points is calculated. Because the coil field is already known, the true material field at the nth iteration is now easily determined as

$$b_{mj}^{(n)} = b_j^{(n)} - b_{cj}^{(n)} \qquad j = 1, \ldots, N_j. \tag{8}$$

The true material field typically differs from the estimate used in (6) and (7); therefore, the constraints (4) are no longer satisfied. However, the difference in the material fields between successive iterations tends to progressively decrease. In practice, the stopping criteria is slightly relaxed so that an excessive number of iterations is avoided, and therefore, the process is repeated until

$$\left| b_{cj}^{(n)} - b_{tj}^{(n)} \right| \leq \gamma \varepsilon B_0 \qquad j = 1, \ldots, N_j \tag{9}$$

where the convergence factor γ is typically chosen between 1 and 3.

B. LP Formulation

At each iteration of the proposed method, we encounter the problem of determining a minimum-volume coil configuration that satisfies the field uniformity constraints (6). To accomplish this task, we begin by segmenting the specified feasible coil domain with a dense grid that defines an array of N_k candidate coils, each of which is located at the center of a grid cell (see Fig. 2). These grid cells do not represent physical cross sections of the candidate coils but, rather, only serve to define their spacing and location.

We can now define the axial magnetic-field matrix $\boldsymbol{A}$, for which the element A_{jk} is the field per unit current at the jth target point due only to the kth candidate coil. This condition allows us to write the matrix expression:

$$\boldsymbol{b_c} = \boldsymbol{Ai} \tag{10}$$

where $\boldsymbol{b_c}$ is the vector of axial coil magnetic fields at the N_j target points, and $\boldsymbol{i}$ is the vector of currents in the N_k coils.

The total conductor volume V in the array of N_k circular coils is given by

$$V = \sum_{k=1}^{N_k} 2\pi r_k S_k \tag{11}$$

where r_k and S_k are the radius and cross section of the kth coil, respectively. Assuming a constant current density of J in all of the candidate coils, the individual currents satisfy

$$|i_k| = JS_k \tag{12}$$

where i_k is the current in the kth coil. Hence, the total volume can be rewritten as

$$V = \frac{2\pi}{J} \sum_{k=1}^{N_k} r_k |i_k|. \tag{13}$$

As pointed out in [14], this expression is valid for any series-connected coil configuration employing a uniform wire size.

Combining (6) and (10), the coil volume minimization problem at the nth iteration may be expressed as

$$\text{Minimize}: \quad \boldsymbol{\Psi} = \sum_{k=1}^{N_k} r_k |i_k| \tag{14a}$$

$$\text{Subject to}: \quad \boldsymbol{b_t}^{(n-1)} - \varepsilon B_0 \leq \boldsymbol{Ai} \leq \boldsymbol{b_t}^{(n-1)} + \varepsilon B_0. \tag{14b}$$

This expression is an ℓ_1-norm minimization problem, which can be rewritten in canonical LP form and solved for the globally optimal currents with the method presented in [14]. One beneficial feature of this problem is that it yields a sparse solution, for which the minimum number of nonzero currents required to satisfy the homogeneity constraints are obtained. In solving the minimization problem (14), we use the built-in function linprog from MATLAB (version 7.11, The MathWorks Inc., Natick, MA), which employs an interior-point predictor–corrector algorithm based on the linear-programming interior-point solvers (LIPSOL) method [41].

When performing the magnetic field calculations required when assembling $\boldsymbol{A}$, we initially approximate each of the candidate coils by an ideal current loop with a zero cross-sectional area. This approach permits the use of simple axial field formulas involving complete elliptic integrals of the first and second kind [42]. When iterating on finer coil grids based on the procedure described in [14], the method in [43] is used to calculate the field due to real coils with finite rectangular cross-sections. The required cross-sectional areas (and dimensions) of the real coils are determined from the optimal currents using an aspect ratio specified by the magnet designer prior to optimization.

The yoke geometry is not included in the aforementioned optimization process. Therefore, the resulting designs obtained with this method are suboptimal. Because the weight and cost of these systems are strongly related to the design of the yoke structure, incorporating the nonlinear optimization of the magnetic materials within this scheme is a subject of future interest.

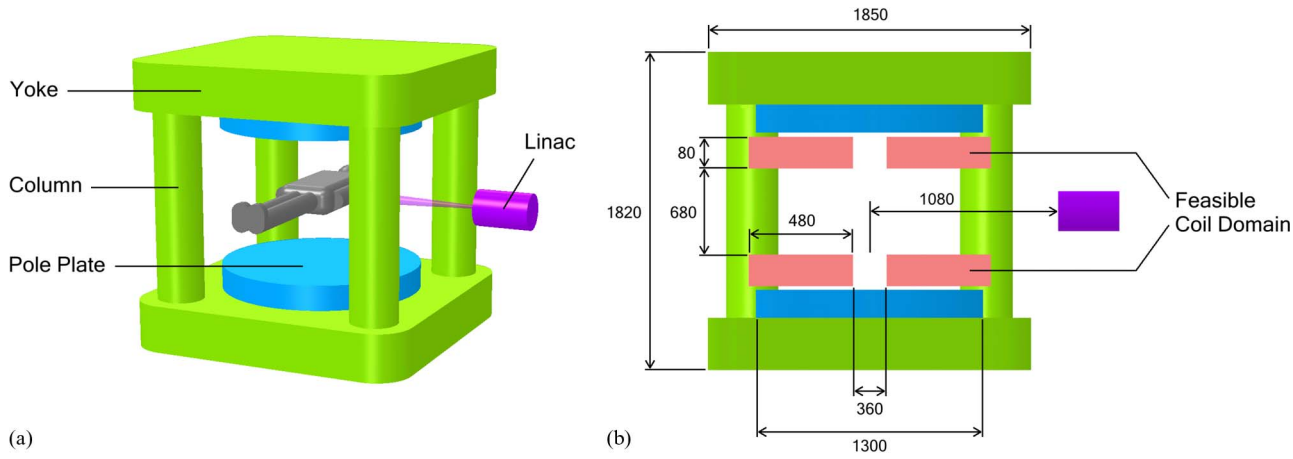

Fig. 3. (a) 3-D schematic of the four-column magnetic yoke structure. (b) Cross-sectional view, with dimensions in millimeters.

III. Optimization Example

The method described in this paper has been applied to the optimal design of an open compact 0.5 T biplanar superconducting magnet assembly for potential use in the linac–MRI system currently pursued by our group [38]–[40]. The geometry of the magnet assembly and linac arrangement is illustrated in Fig. 3.

This system is designed to employ a conduction-cooled cryogen-free coil configuration constructed from a MgB_2 HTS material. In the absence of any liquid coolant, we eliminate the requirement of a bulky cryostat vessel that consists of a safety ventilation system, thereby making the mechanical rotation of the entire scanner feasible.

An operating coil temperature of approximately 12 K could be achieved using two double-stage Gifford–McMahon (GM) cryocooler subassemblies in a conduction-cooled split cryostat design similar to the designs detailed in [44] and [45]. Within a vacuum chamber that encompasses each of the magnet poles, a thermal screen that surrounds the superconducting coil arrangement would be thermally coupled to the first stage of a single GM cryocooler. The second stage of this cryocooler could then be coupled to a set of thermally conductive rings and sheets embedded within and bonded adjacent to the coil forms and windings. It is expected that such a crysostat design and associated support structures would occupy an additional 3–4 cm of space surrounding the coils. By employing superconducting joints recently developed for MgB_2 tapes [46], this design permits a persistent mode of operation.

A realistic target for the engineering critical current density for MgB_2 is 28 kA/cm^2 at 12 K and 4 T [24]. Based on this value, we specify a working current density of 21 kA/cm^2 at approximately 75% of the critical value.

The outer dimensions of the four-column yoke structure illustrated in Fig. 3 have been chosen to permit the rotation of the magnet assembly within a typical radiotherapy vault of a 3 m height. In particular, a practical clearance of 40 cm is achieved for the magnet to allow room for additional peripheral equipment [36], [37]. The remaining dimensions were selected such that the total weight of magnetic material was within 10% of the 20 t yoke structure used in a commercially available

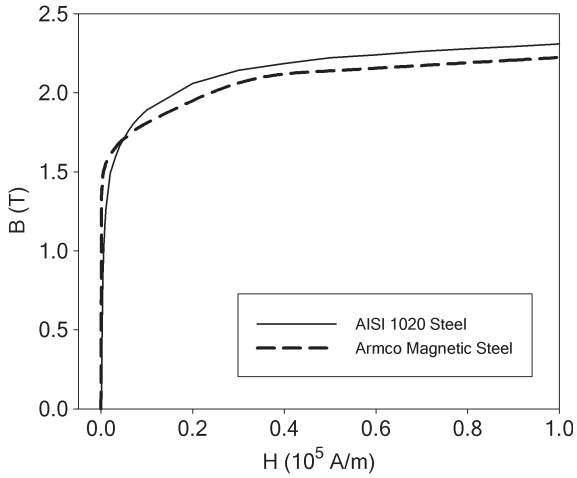

Fig. 4. Nonlinear magnetization curves for AISI 1020 plain carbon steel and Armco magnetic steel.

conduction-cooled 0.5 T biplanar system with an acceptable fringe magnetic field [47].

The yoke and column structures of the magnet assembly are composed of AISI 1020 plain carbon steel, and the pole plates are composed of special Armco magnetic steel. The nonlinear magnetization curves for these materials are shown in Fig. 4 [48], [49].

The feasible coil domain is defined in the region surrounding the pole plates such that adequate space is supplied for the cooling and mounting system while providing a patient gap of approximately 60 cm (see Fig. 3). An initial array of 192 circular candidate coils with a grid spacing of 2 cm is employed. This grid spacing is further reduced to 1–2 mm during the refinement process in the LP coil optimization method [14]. Because the coil configuration in this particular magnet design is completely axisymmetric, only axisymmetric field inhomogeneities may be constrained. Accordingly, a distribution of 34 target points is defined along a single polar arc located on the surface of a 40 cm DSV at the isocenter, as shown in Fig. 5.

Once the minimum-volume coil configuration at each iteration is obtained, a FEM model is generated and analyzed to determine the complete magnetic fields produced by the

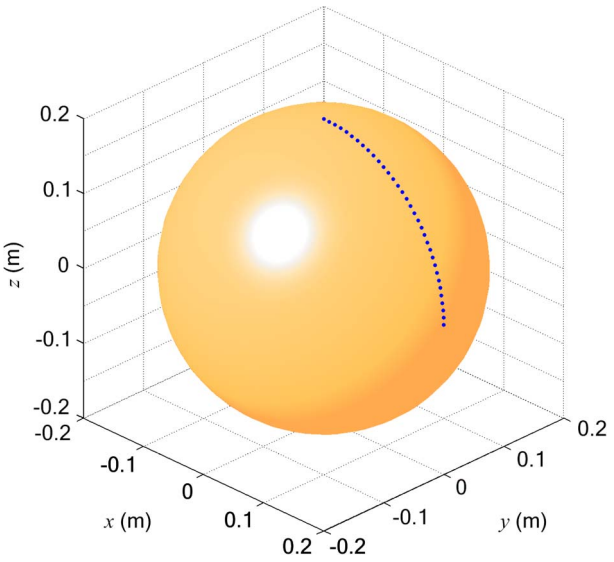

Fig. 5. Target point distribution on the surface of a 40 cm DSV at the isocenter.

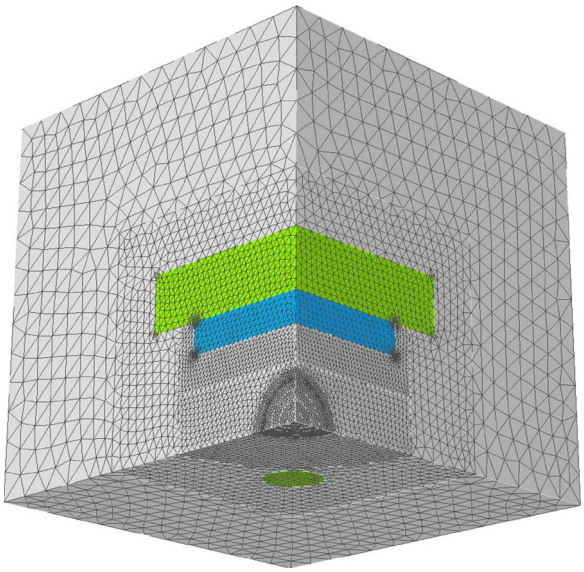

Fig. 6. Simplified FEM model geometry and mesh, excluding conductors. The entire modeling domain that extends far from the isocenter is only partially shown for clarity.

entire magnet assembly. In our current implementation, we use the 3-D FEM software package Opera-3d (version 13.0, Cobham plc, Wimborne Minster, England), which employs the magnetostatics solver TOSCA to calculate the scalar magnetic potential and magnetic field values at discrete points within the model geometry [50]. The updated parameters that define the coil configuration are passed to Opera-3d using a component object model (COM) interface that is established within the MATLAB script. This way, updating the complete FEM model at each iteration is an automated step in the optimization. Due to symmetry, only 1/8 of the magnet structure is included in the model geometry, which is partitioned with 1.017×10^6 tetrahedral quadratic Lagrange elements. The simplified model geometry and FEM mesh is shown in Fig. 6.

When executing the optimization method, the target field B_0 is set to 0.5 T, with a relative field error ε of 10^{-5} and a

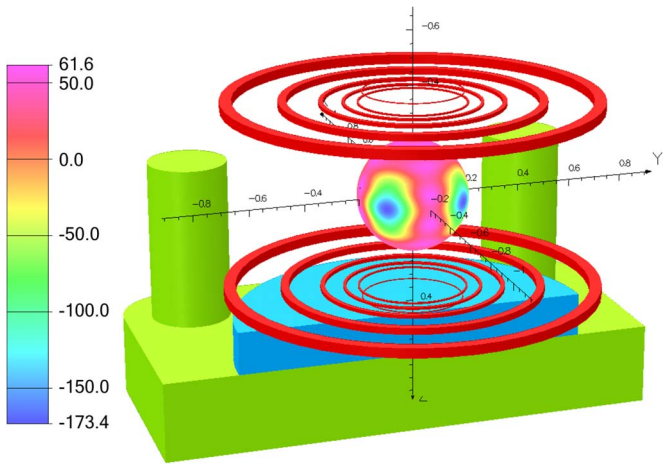

Fig. 7. Complete optimal coil configuration. The axial magnetic field variation (in parts per million) is plotted over the surface of a 40 cm DSV at the isocenter. Only a quarter section of the yoke geometry is shown for clarity. Axis dimensions are given in meters.

TABLE I
OPTIMIZED COIL CONFIGURATION

Coil	Radial position (mm)	Axial position (mm)	Radial width (mm)	Axial width (mm)	Current (kA·turns)
1	181.1	381.1	3.7	3.1	-2.416
2	194.4	341.1	6.7	5.6	7.909
3	245.6	341.1	10.8	9.0	-20.416
4	324.9	341.1	16.4	13.6	46.888
5	461.1	341.1	29.5	24.6	-152.608
6	658.9	341.1	42.7	35.6	319.034

Due to symmetry, only the dimensions for the upper pole are shown.

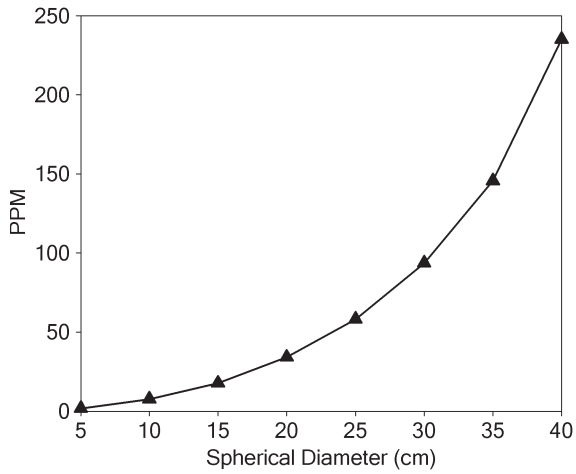

Fig. 8. Total peak-to-peak axial magnetic field inhomogeneity measured in parts per million as a function of the DSV size.

convergence factor γ of 2, resulting in an expected peak-to-peak field error of at most 40 ppm at the target points in the final design.

The optimal magnet design illustrated in Fig. 7 is obtained in 11 iterations. The dimensions of the resulting coil configuration are detailed in Table I. The total conductor volume in the 12 circular coils is 1.791×10^4 cm^3. A central magnetic field

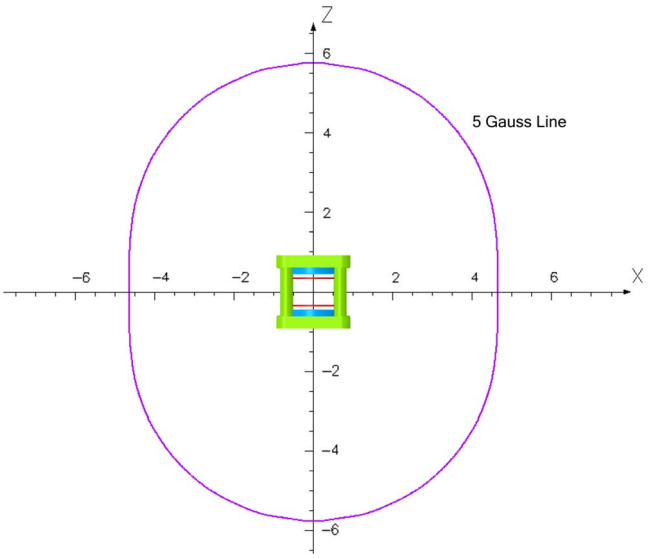

Fig. 9. Fringe field extent of the optimized magnet. The 5 G magnetic-field line is plotted in the xz plane. Axis dimensions are given in meters.

TABLE II
SPHERICAL HARMONIC DECOMPOSITION OF THE AXIAL MAGNETIC-FIELD INHOMOGENEITY

Order	Degree	Harmonic amplitude (ppm)
2	0	115
4	0	-52
4	4	98
6	0	18
6	4	-21
8	0	1
8	4	1
10	0	20
12	0	-45
14	0	-2
16	0	5

Amplitudes calculated over a 40 cm DSV.

strength of 0.500 T is achieved, and the peak-to-peak axial field inhomogeneity is 26.1 ppm at the target points, therefore satisfying the specified design constraints. The total inhomogeneity over the entire 40 cm DSV is 235.0 ppm, which is inherently limited by the nonaxisymmetric nature of the yoke structure. A result of this magnitude is typical for the theoretical design of biplanar magnets with nonaxisymmetric yoke geometries [51], [52], for which achieving a uniform magnetic field is generally more difficult than with a cylindrical magnet. The use of postmanufacturing shimming techniques would be necessary to further reduce the remaining inhomogeneities to a level suitable for medical imaging.

The total inhomogeneity as a function of the DSV size is shown in Fig. 8, and the extent of the fringe field is shown in Fig. 9. The peak field at the coils is 3.428 T, which satisfies the specifications for the conductor material chosen. For completeness, the harmonic amplitudes for the spherical harmonic decomposition of the axial magnetic field inhomogeneity over a 40 cm DSV at the isocenter are provided in Table II.

It has been demonstrated that the linac waveguide is sensitive to the transverse magnetic fields that it experiences at the location illustrated in Fig. 3 [53]. Accordingly, additional linear constraints similar to the constraints in (1) could be defined such that the strength of the magnetic field along the linac would be limited during the aforementioned optimization process. Shielding the linac with this approach would require an increase in the coil currents and would result in higher peak fields. Hence, simpler alternative approaches involving a dedicated shielding system are preferred [54].

IV. CONCLUSION

An iterative method has been presented for the optimal design of homogenous superconducting MRI systems that contain magnetic materials. In addition to minimizing the conductor volume, one key feature of this method is its ability to handle magnet designs involving complicated noncylindrical magnetic yoke geometries, such as those found in modern passively shielded biplanar MRI scanners. The accurate design of these systems requires the use of computationally expensive numerical techniques for the magnetic field analysis, the burden of which is alleviated by the rapid convergence achieved with the proposed method.

REFERENCES

[1] A. Ishiyama, M. Hondoh, N. Ishida, and T. Onuki, "Optimal design of MRI magnets with magnetic shielding," *IEEE Trans. Magn.*, vol. 25, no. 2, pp. 1885–1888, Mar. 1989.
[2] A. Ishiyama, T. Yokoi, S. Takamori, and T. Onuki, "An optimal design technique for MRI superconducting magnets using mathematical programming method," *IEEE Trans. Magn.*, vol. 24, no. 2, pp. 922–925, Mar. 1988.
[3] M. Fujita, "The coil design of the superconducting MRI magnet," *IEEE Trans. Magn.*, vol. 24, no. 6, pp. 2907–2909, Nov. 1988.
[4] S. Pissanetzky, "Structured coils for NMR applications," *IEEE Trans. Magn.*, vol. 28, no. 4, pp. 1961–1968, Jul. 1992.
[5] M. R. Thompson, R. W. Brown, and V. C. Srivastava, "An inverse approach to the design of MRI main magnets," *IEEE Trans. Magn.*, vol. 30, no. 1, pp. 108–112, Jan. 1994.
[6] S. Crozier and D. M. Doddrell, "Compact MRI magnet design by stochastic optimization," *J. Magn. Reson.*, vol. 127, no. 2, pp. 233–237, Aug. 1997.
[7] P. N. Morgan, S. M. Conolly, and A. Macovski, "Resistive homogeneous MRI magnet design by matrix subset selection," *Magn. Reson. Med.*, vol. 41, no. 6, pp. 1221–1229, Jun. 1999.
[8] S. Crozier, H. Zhao, and D. M. Doddrell, "Current density mapping approach for design of clinical magnetic resonance imaging magnets," *Conc. Magn. Reson.*, vol. 15, no. 3, pp. 208–215, Oct. 2002.
[9] N. R. Shaw and R. E. Ansorge, "Genetic algorithms for MRI magnet design," *IEEE Trans. Appl. Supercond.*, vol. 12, no. 1, pp. 733–736, Mar. 2002.
[10] G. Sinha, R. Sundararaman, and G. Singh, "Design concepts of optimized MRI magnet," *IEEE Trans. Magn.*, vol. 44, no. 10, pp. 2351–2360, Oct. 2008.
[11] M. Xu, M. Ogle, X. Huang, K. Amm, and E. T. Laskaris, "Iterative EM design of an MRI magnet using HTS materials," *IEEE Trans. Appl. Supercond.*, vol. 17, no. 2, pp. 2192–2195, Jun. 2007.
[12] Y. Lvovsky and P. Jarvis, "Superconducting systems for MRI-present solutions and new trends," *IEEE Trans. Appl. Supercond.*, vol. 15, no. 2, pp. 1317–1325, Jun. 2005.
[13] A. K. Kalafala, "A design approach for actively shielded magnetic resonance imaging magnets," *IEEE Trans. Magn.*, vol. 26, no. 3, pp. 1181–1188, May 1990.

[14] H. Xu, S. M. Conolly, G. C. Scott, and A. Macovski, "Homogeneous magnet design using linear programming," *IEEE Trans. Magn.*, vol. 36, no. 2, pp. 476–483, Mar. 2000.
[15] V. Cavaliere, A. Formisano, R. Martone, and M. Primizia, "A genetic algorithm approach to the design of split coil magnets for MRI," *IEEE Trans. Appl. Supercond.*, vol. 10, no. 1, pp. 1376–1379, Mar. 2000.
[16] V. Cavaliere, A. Formisano, R. Martone, G. Masullo, A. Matrone, and M. Primizia, "Design of split coil magnets for magnetic resonance imaging," *IEEE Trans. Appl. Supercond.*, vol. 10, no. 1, pp. 759–762, Mar. 2000.
[17] J. H. Jensen, "Minimum-volume coil arrangements for generation of uniform magnetic fields," *IEEE Trans. Magn.*, vol. 38, no. 6, pp. 3579–3588, Nov. 2002.
[18] S. Besio, S. Pittaluga, V. Punzo, and A. Trequattrini, "Elliptical coils for dedicated MRI magnets," *IEEE Trans. Appl. Supercond.*, vol. 18, no. 2, pp. 908–911, Jun. 2008.
[19] Q. M. Tieng, V. Vegh, and I. M. Brereton, "Globally optimal superconducting magnets—Part I: Minimum stored energy (MSE) current density map," *J. Magn. Reson.*, vol. 196, no. 1, pp. 7–11, Jan. 2009.
[20] Q. M. Tieng, V. Vegh, and I. M. Brereton, "Globally optimal superconducting magnets—Part II: Symmetric MSE coil arrangement," *J. Magn. Reson.*, vol. 196, no. 1, pp. 7–11, Jan. 2009.
[21] Q. Wang, G. Xu, Y. Dai, B. Zhao, L. Yan, and K. Kim, "Design of open high-magnetic-field MRI superconducting magnet with continuous current and genetic algorithm method," *IEEE Trans. Appl. Supercond.*, vol. 19, no. 19, pp. 2289–2292, Jun. 2009.
[22] Q. M. Tieng, V. Vegh, and I. M. Brereton, "Minimum stored energy high-field MRI superconducting magnets," *IEEE Trans. Appl. Supercond.*, vol. 19, no. 4, pp. 3645–3652, Aug. 2009.
[23] C. Wang, Q. Wang, and Q. Zhang, "Multiple-layer superconducting magnet design for magnetic resonance imaging," *IEEE Trans. Appl. Supercond.*, vol. 20, no. 3, pp. 706–709, Jun. 2010.
[24] S. Pittaluga, S. Besio, V. Punzo, and A. Trequattrini, "Racetrack coils for dedicated MRI magnets," *IEEE Trans. Appl. Supercond.*, vol. 20, no. 3, pp. 786–789, Jun. 2010.
[25] M. Kitamura, S. Kakukawa, K. Mori, and T. Tominaka, "An optimal design technique for coil configurations in iron-shielded MRI magnets," *IEEE Trans. Magn.*, vol. 30, no. 4, pp. 2352–2355, Jul. 1994.
[26] H. Siebold, H. Huebner, L. Soeldner, and T. Reichert, "Performance and results of a computer program for optimizing magnets with iron," *IEEE Trans. Magn.*, vol. 24, no. 1, pp. 419–422, Jan. 1988.
[27] M. D. Ogle and J. DAngelo, "Design optimization method for a ferromagnetically self-shield MR magnet," *IEEE Trans. Magn.*, vol. 27, no. 2, pp. 1689–1691, Mar. 1991.
[28] V. E. Eregin, V. S. Kashikhin, A. A. Lipatnikov, Y. P. Severgin, V. P. Shangin, and N. A. Shatil, "Formation of homogeneous field in a shielded superconducting solenoid for an MRI," *IEEE Trans. Magn.*, vol. 28, no. 1, pp. 675–677, Jan. 1992.
[29] S. Noguchi and A. Ishiyama, "Optimal design method for MRI superconducting magnets with ferromagnetic shield," *IEEE Trans. Magn.*, vol. 33, no. 2, pp. 1904–1907, Mar. 1997.
[30] H. Zhao and S. Crozier, "Rapid field calculations for the effect of ferromagnetic material in MRI magnet design," *Meas. Sci. Technol.*, vol. 13, no. 2, pp. 198–205, Feb. 2002.
[31] H. Zhao and S. Crozier, "A design method for superconducting MRI magnets with ferromagnetic material," *Meas. Sci. Technol.*, vol. 13, no. 12, pp. 2047–2052, Dec. 2002.
[32] Y. Muruta, M. Abe, R. Ando, and T. Nakayama, "A novel design method of shapes of ferromagnetic materials for the superconducting MRI magnets," *IEEE Trans. Appl. Supercond.*, vol. 19, no. 3, pp. 2293–2296, Jun. 2009.
[33] X. Tang, D. Zu, T. Wang, and B. Han, "An optimizing design method for a compact iron-shielded superconducting magnet for use in MRI," *Supercond. Sci. Technol.*, vol. 23, no. 8, pp. 085008-1–085008-6, Aug. 2010.
[34] C. Wu, J. Guo, C. Chen, G. Yan, and C. Li, "Optimal design and test of main magnet in superconducting MRI," *IEEE Trans. Appl. Supercond.*, vol. 20, no. 3, pp. 1810–1813, Jun. 2010.
[35] M. W. Garrett, "Axially symmetric systems for generating and measuring magnetic fields," *J. Appl. Phys.*, vol. 22, no. 9, pp. 1091–1107, Sep. 1951.
[36] T. Tadic and B. G. Fallone, "Design and optimization of a novel bored biplanar permanent magnet assembly for hybrid MRI systems," *IEEE Trans. Magn.*, vol. 46, no. 12, pp. 4052–4058, Dec. 2010.
[37] T. Tadic and B. G. Fallone, "Three-dimensional nonaxisymmetric pole piece shape optimization for biplanar permanent magnet MRI systems," *IEEE Trans. Magn.*, vol. 47, no. 1, pp. 231–238, Jan. 2011.
[38] B. G. Fallone, M. Carlone, B. Murray, S. Rathee, T. Stanescu, S. Steciw, K. Wachowicz, and C. Kirkby, "Development of a linac-MRI system for real-time ART," *Med. Phys.*, vol. 34, no. 6, p. 2547, Jun. 2007.
[39] B. G. Fallone, B. Murray, S. Rathee, T. Stanescu, S. Steciw, and S. Vidakovic, "First MR images obtained during megavoltage photon irradiation from a prototype integrated linac-MR system," *Med. Phys.*, vol. 36, no. 6, pp. 2084–2088, Jun. 2009.
[40] B. G. Fallone, "Real-time MR-guided radiotherapy: Integration of a low-field MR system," *Med. Phys.*, vol. 36, no. 6, pp. 2774–2775, Jun. 2009.
[41] Y. Zhang, "Solving large-scale linear programs by interior-point methods under the Matlab environment," *Optim. Methods Softw.*, vol. 10, no. 1, pp. 1–31, 1998.
[42] D. B. Montgomery, *Solenoid Magnet Design*. New York: Wiley-Interscience, 1969.
[43] L. K. Forbes, S. Crozier, and D. M. Doddrell, "Rapid computation of static fields produced by thick circular solenoids," *IEEE Trans. Magn.*, vol. 33, no. 5, pp. 4405–4410, Sep. 1997.
[44] D. Damiani, A. Laurenti, R. Marabotto, and M. P. Segre, "Coil with superconductive windings cooled without cryogenic fluids," U.S. Patent 8 022 798 B2, Sep. 20, 2011.
[45] E. T. Laskaris, R. Ackermann, B. Dorri, D. Gross, K. Herd, and C. Minas, "A cryogen-free open superconducting magnet for interventional MRI applications," *IEEE Trans. Appl. Supercond.*, vol. 5, no. 2, pp. 163–168, Jun. 1995.
[46] D. Nardelli, R. Marabotto, and A. Laurenti, "Superconducting Coil Having a Granular Superconducting Junction," Publication EP 2 286 488 A1, Feb. 23, 2011.
[47] M. Razeti, S. Angius, L. Bertora, D. Damiani, R. Marabotto, M. Modica, D. Nardelli, M. Perrella, and M. Tassisto, "Construction and operation of cryogen-free MgB_2 magnets for open MRI systems," *IEEE Trans. Appl. Supercond.*, vol. 18, no. 2, pp. 882–886, Jun. 2008.
[48] N. B. S. Gloria, M. C. L. Areiza, I. V. J. Miranda, and J. M. A. Rebello, "Development of a magnetic sensor for detection and sizing of internal pipeline corrosion defects," *NDT&E Int.*, vol. 42, no. 8, pp. 669–677, Dec. 2009.
[49] D. M. Kohler, "Production and properties of grain-oriented commercially pure iron," *J. Appl. Phys.*, vol. 38, no. 3, pp. 1176–1178, Mar. 1967.
[50] *Opera-3D Reference Manual*, ver. 13.014, Comsol AB, Stockholm, Sweden, 2009.
[51] X. Jiang, G. Shen, Y. Lai, and J. Tian, "Development of an open 0.3-T NdFeB MRI magnet," *IEEE Trans. Appl. Supercond.*, vol. 14, no. 2, pp. 1621–1623, Jun. 2004.
[52] J. S. Ryu, Y. Yao, C. S. Koh, and Y. J. Shin, "3-D optimal shape design of pole piece in permanent magnet MRI using parameterized nonlinear design sensitivity analysis," *IEEE. Trans. Magn.*, vol. 42, no. 4, pp. 1351–1354, Apr. 2006.
[53] J. St. Aubin, S. Steciw, and B. G. Fallone, "Effect of transverse magnetic fields on a simulated in-line 6-MV linac," *Phys. Med. Biol.*, vol. 55, no. 16, pp. 4861–4869, Aug. 2010.
[54] J. St. Aubin, S. Steciw, and B. G. Fallone, "Magnetic decoupling of the linac in a low-field biplanar linac-MR system," *Med. Phys.*, vol. 37, no. 9, pp. 4755–4761, Sep. 2010.

Tony Tadic was born in Edmonton, AB, Canada in 1984. He received the B.Sc. degree in engineering physics in 2006 from the University of Alberta, Edmonton, AB, Canada, where he is currently working toward the Ph.D. degree in medical physics in the Department of Physics, in collaboration with the Medical Physics Department, Cross Cancer Institute, Edmonton.

He is a Member of the ART^2 Research Group, Cross Cancer Institute, where efforts are being made to develop the world's first hybrid integrated medical linear accelerator and magnetic resonance imager.

Mr. Tadic is a Student Member of the American Association of Physicists in Medicine and the Canadian Organization of Medical Physicists.

B. Gino Fallone, biography not available at the time of publication.